Mechanical behaviour and interface evaluation of hybrid MIM/PBF stainless steel components

Mehmeti, Aldi; Penchev, Pavel; Lynch, Donal; Vincent, Denis; Maillol, Nathalie; Maurath, Johannes; Bajolet, Julien; Wimpenny, David; Essa, Khamis; Dimov, Stefan

DOI:
10.1108/RPJ-10-2019-0256

Document Version
Peer reviewed version

Citation for published version (Harvard):
Mehmeti, A, Penchev, P, Lynch, D, Vincent, D, Maillol, N, Maurath, J, Bajolet, J, Wimpenny, D, Essa, K & Dimov, S 2020, 'Mechanical behaviour and interface evaluation of hybrid MIM/PBF stainless steel components', *Rapid Prototyping Journal*, vol. 26, no. 10, pp. 1809-1825. https://doi.org/10.1108/RPJ-10-2019-0256

Mechanical Behaviour and Interface Evaluation of Hybrid MIM/PBF Stainless Steel Components

Aldi Mehmeti[1], Pavel Penchev[1], Donal Lynch[1], Denis Vincent[2], Nathalie Maillol[3], Johannes Maurath[4], Julien Bajolet[3], David Wimpenny[5], Khamis Essa[1], Stefan Dimov[1]

[1] School of Mechanical Engineering, University of Birmingham, Edgbaston, Birmingham B15 2TT, UK

[2] Université Grenoble Alpes, F-38000 Grenoble, France; CEA, LITEN, DTNM, SERE, LRVM, F-38054 Grenoble, France

[3] IPC, Oyonnax, France

[4] MIMplus Technologies, Germany

[5] MTC, Coventry, UK

Abstract

The manufacture of hybrid components, especially by combining the capabilities of Additive Manufacturing (**AM**) processes with cost-effective complementary technologies, has attracted the attention of industry and researchers because they can offer flexibility and cost advantages in producing small series of customisable products. The paper reports an investigation into the mechanical behaviour of hybrid components produced by combining the capabilities of Metal Injection Moulding (**MIM**) with the laser-based Powder Bed Fusion (PBF) process to produce small series of hybrid components. In particular, the MIM process is employed to fabricate relatively lower cost preforms in higher quantities while the PBF technology is deployed to build on them sections that can be personalised, customised or functionalised to meet specific technical requirements. The research investigates systematically the mechanical properties and the performance of the MIM/PBF interfaces in such hybrid components. The results are discussed, and conclusions are made about the mechanical performance of such hybrid components produced in batches and also about the production efficiency of the investigated hybrid manufacturing (**HM**) route.

1. Introduction

Manufacturing industry is highly competitive and the innovation there is driven by several factors including cost, efficiency, product performance and increasingly environmental impact. Also, there is a trend manufacturers to produce various configurations of same components based on common generic designs that are then customised/functionalised for ranges of products or according to customers specific requirements [1] [2]. The necessity for unconstrained production in smaller series with increased productivity, design flexibility, assemblability and surface durability in different environments, among others should also satisfy strong economic

constraints [3] [4]. Subsequently, in parallel to the demand for high value innovative components that meet the constantly increasing requirements for production efficiency there is a common denominator, the growing legislative pressure for sustainability and a lower environmental impact [5].

Therefore, to produce and/or reproduce metal components in small series, several manufacturing processes have been employed over the years, such as machining, (MIM) and more recently (AM) and (HM). All these technologies have some advantages but also limitations regarding production efficiency, manufacturing costs and achievable geometries. Furthermore, dimensional accuracy, geometrical complexity, surface integrity and mechanical properties of the produced components vary greatly across these technologies and are important considerations in determining their capabilities and interoperability when integrating them in a process chain or production line. In particular, the interfaces of these manufacturing processes with any pre- and post-processing technologies should be taken into account when integrating them and so to meet the technical requirements and any cost constraints associated with a given application [6]. In addition, their technological limitations should be considered, too, i.e. their ability to process only certain materials and achievable geometrical complexity, together with required capital investment and thus to determine their cost-effective application areas [7].

The machining technology has a significant advantage because of the high precision and repeatability that can be achieved and the flexibility that it offers. However, it is also associated with high amount of material waste and difficulties in processing complex geometries and materials with high hardness [8]. As a result, this can increase processing time and production costs while there can be an impact on cutting tool life. Especially, the machining of such high performance materials can lead to excessive tool wear that can impair the tools' efficiency and often can lead to scraping high value components because of poor surface integrity and inability to meet technical requirements of a given application [9][10]. Additionally, the necessary cutting tool access to processed surfaces makes difficult and, in many cases, impossible the machining of geometries with internal features. This can be due to tool shape limitations and available machine tool configurations and degrees of freedom that often can result in interferences between machine tool/cutting tool shanks-holders and processed geometries. Ultimately, the necessity to manage and potentially to minimise the impact of these constrains leads to requirements for validation of the machining strategies through the use of time consuming and expensive simulations and thus to generate collision free toolpaths [11].

At the same time, metal AM technologies have attracted a significant industrial interest due to advantages in regards to their production scalability, design freedom, capabilities to produce complex geometries, e.g. internal cooling channels, topologically optimised geometries and organic-lattice shapes, while the main processing principals are relatively simple, i.e. an incremental layer-by layer collision free manufacturing [12][13][14]. However, they have some intrinsic limitations, too, such as: the lack of data preparation tools for achieving a fully digital information data flow between design, machining, AM processes and other post-processing steps [15]; AM components suffer from the stair-step effect due to their layer-wise built strategies; they are energy based processes that introduce constraints regarding achievable surface integrity and geometrical accuracy and therefore post processing is considered compulsory[16] [17] [18]; microstructural inconsistencies between layers [19]; and last but not the least, metallurgical defects due to gas entrapments and partially fused powders that lead to porosities and residual stresses that undermine the mechanical properties of the produced components[20] [21].

The other well-established option is the MIM technology. However, it is a viable proposition for producing relatively large number of components. The process is also employed for producing components that are difficult or impossible to machine due to some intricate geometries, thin walls/structures and high material hardness [22][23]. Moreover, the surface quality of produced components is relatively high, i.e. surface roughness R_a < 1.2 μm, and therefore in many cases post-processing operations are not required [24]. Despite these advantages, the MIM technology has some limitations, too, that should be considered when planning the production processes, i.e. the tight tolerances and high surface smoothness of the produced parts are highly dependent on the mould's surfaces,

the component geometry and feedstocks [25]. The required tooling entails high initial costs that increases the lead time and the overall production cost and as such viable product series are usually in the range of thousands. Furthermore, components with flat surfaces or complex geometries exhibit great adhesion onto inner contours due to the shrinkage during cooling and therefore the moulds should incorporate draft angles to assist their release. So, the final product geometry should be altered slightly in order to address such manufacture requirements. In addition, this is a replication process in its nature and therefore any design changes entail mould modifications or completely new tools. Thus, this technology is not so flexible as machining and AM processes and the unit cost increases quickly when the product series are reduced [22][26].

The other option that has attracted a significant industrial interest recently are HM processes because of their capabilities to combine two or more processes synergistically in a single setup. Thus, to address the limitations of its constituent technologies while there are less constraints concerning the components' design[27][28] [29][30][31]. However, despite their high manufacturing flexibility, the HM machine tools also do have some important limitations arising from the integration of processes with fundamentally different physical characteristics in a single machine setup. For example, a HM system that combines AM technology, i.e. a direct energy deposition (DED) technology, with precision milling in a single machine tool has to meet the operating conditions of both processes. Furthermore, combining the DED and milling technologies introduces another issue regarding the powder and swarf managements, and the necessity of completely different auxiliary sub-systems, e.g. for controlling the DED environment and specific work-holding sub-systems to withstand the cutting forces during the milling operations. In addition, the productivity and cost effectiveness of HM systems is greatly reduced because the integration of processes in a single set-up allows only one manufacturing technology to be active at a time. Lastly, as it was the case with standalone AM processes the existence of metallurgical defects in the deposited material can also significantly impair the parts' mechanical properties [21].

Considering the limitations of all standalone processes the research community and industries turned their attention to multi-setup manufacturing solutions, also referred to as process chains or production lines, to combine the capabilities of complementary manufacturing processes sequentially [32]. In this way each constituent processes in such solutions can be optimised to address the specific performance requirements of an individual technology as it is the case in standalone processes. So, the physical characteristics of integrated processes does not change and therefore the overall cost does not increase considerably, compared to the single setup HM systems. In addition, the productivity is increased due to the parallel utilisation of constituent processes while they still have the flexibility to synchronise their throughputs with other integrated processes. There are significant advances in system level tools for integration of AM processes, e.g. powder bed fusion (PBF) technologies [15] [33], in multi-setup HM platforms for producing hybrid components[34].

Although the manufacture of hybrid components has attracted the attention of industry and researchers, their mechanical characteristics have not been extensively studied. Notably, most of reported research is theoretical or focused on a specific application, e.g. repair of tools and high value components, and not on developing hybrid components for new products and on issues associated with their scale up manufacture [2][35][36][37]. Usually, the reported research is limited to the fabrication of one hybrid component and not on their batch manufacture whilst the underpinning methodologies cannot support their serial production [38]. The selection of a suitable AM process for producing high performance components while increasing the production rates and reducing the production cost is critical in developing multi-setup HM platforms. The processing efficiency of AM processes is much lower while the cost per hour much higher than those of subtractive or replication technologies [39] [40] . Therefore, this should be considered carefully when the process plans for producing hybrid components are designed. In particular, the AM processes should be employed for producing only those sections/geometries of the hybrid components that cannot be produced by other processes, e.g. topologically optimised ones [41]. For example, some preforms can be produced in large quantities by employing conventional processes, e.g. machining and MIM, and then customised through metal AM processes. In this way, each process integrated in a multi-setup

HM platform will be used in its cost-effective processing window and thus small batches of high-value hybrid components can be produced.

In this context, the aim of this research is to investigate the mechanical characteristics of hybrid components produced by combining the capabilities of the MIM process, i.e. to produce relatively lower cost preforms in higher quantities, with an AM process, i.e. the PBF process, to personalize, customize or functionalize them. Functionality and performance of such hybrid components were investigated through mechanical tests, metallographic and hardness analyses of their interfaces. The results are discussed, and conclusions are made about the mechanical performance of such hybrid components produced in batches and also about the production efficiency of the proposed HM route.

2. Materials and methods

2.1 Test part and fixture design for batch processing

The test part was selected to be sufficiently small to allow batches of them, i.e. arrays of parts, to be produced and thus to investigate the process consistency in producing hybrid components. The selected test part is a solid tensile bar that can be produced easily with the typical/expected quality of MIM parts and thus can be used directly to investigate the mechanical properties and the interface performance of hybrid MIM/PBF components as shown in Figure 1. The test part dimensions were determined by taking into account the capabilities of the MIM process, especially the bars' thickness was chosen to be less than 2 mm to minimize the shrinkage and also potential distortion of the MIM preforms. The length of the test parts was also reduced to minimize the PBF build time, yet ensuring that they should be able to be clamped adequately in the tensile testing machine and allow for any additional device to be attached and used between the grips, e.g. an extensometer. All together, the selected design had a relatively small cross section area (interface) and thus any misalignments between MIM preforms and PBF sections would impact the mechanical performance of the produced hybrid components.

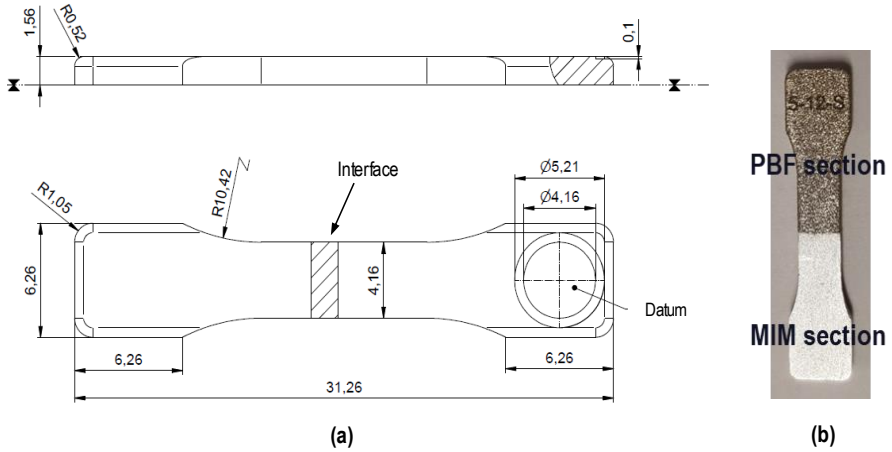

Figure 1: The design of the tensile bar used as a test part all dimensions in mm (a), together with an actual hybrid part (b).

The importance of positioning and fixing the test parts, i.e. MIM preforms, into the PBF system is critical for any batch manufacture, in particular any displacements will result in offsets between the preforms and the built PBF sections. Furthermore, if the preforms are not properly fixed onto the PBF build platform, they can be displaced during the recoating step in the powder bed. Therefore, to produce hybrid components with the required geometrical accuracy and precision, there is a need to design and implement fixtures that can be used as

”adapters” to the system level tools developed for integration of PBF systems into process chains and production lines [15]. In addition, as the hybrid components should be produced in batches, the fixtures should be designed to fix quickly and accurately arrays of test parts. To fulfil these requirements, a fixture was designed to hold 20 MIM preforms and thus to be able to produce batches of hybrid components in each PBF build. The design of this fixture is shown in Figure 2.

The fixture includes a stationary base and two moving jaws with slots that hold the preforms firmly during the PBF operation. The stationary base is fixed to a pallet or a PBF build plate of the modular workpiece holding device via 2 M6 bolts [15] as shown in the exploded view in Figure 2(a), while M4 bolts are used to fix the moving jaws to the stationary base and thus to provide the necessary clamping force for holding the MIM preforms firmly Figure 2(b).In total, five custom fixtures were produced for batch manufacture of hybrid components. The slots were numbered to reference any hybrid components produced in a given PBF build.

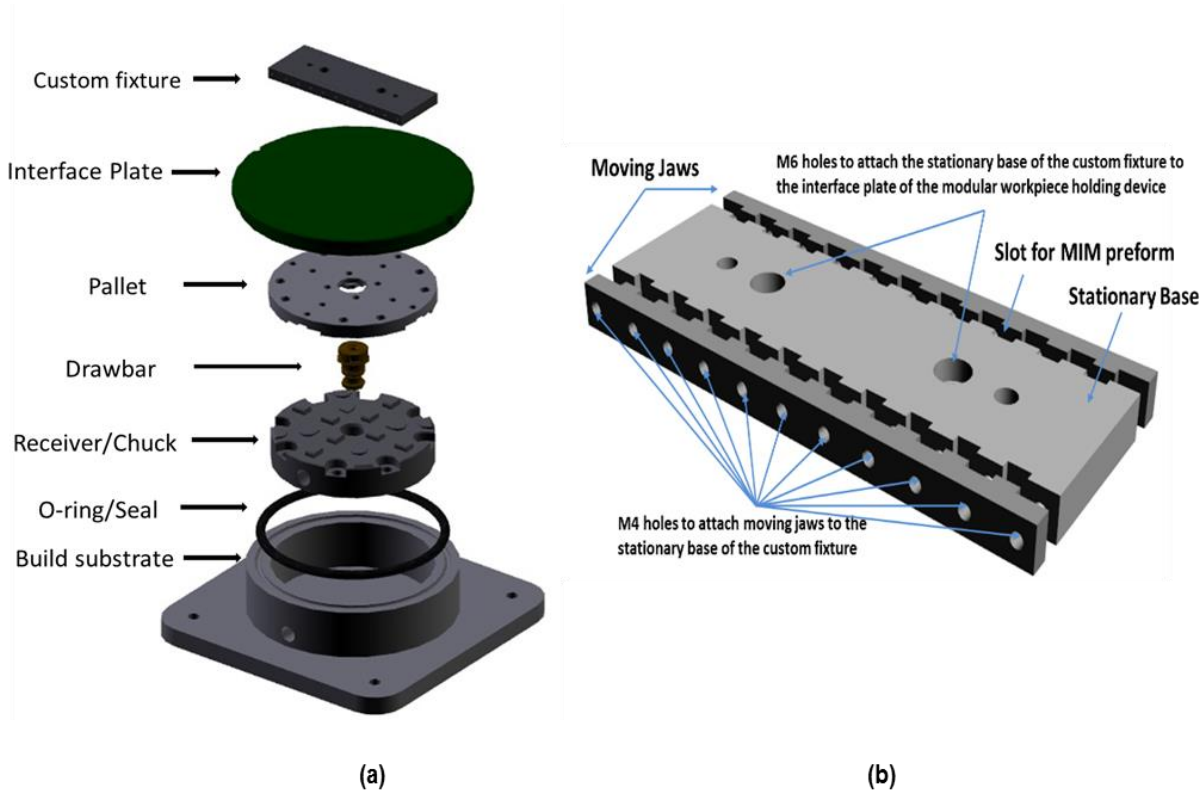

Figure 2. The modular workpiece holding device (a) together with custom fixture for holding 20 MIM preforms during the PBF process (b).

2.2 Multi-setup manufacturing of hybrid components

Hybrid MIM/PBF components were produced employing the custom fixture described in Section 2.1 and specially developed system level tools for integrating PBF systems in process chains and production lines [15]. First, MIM preforms were produced using the established MIMplus technology [42] from feedstocks of three different gas atomized 316L stainless steel powders supplied by Sandvik, EOS and a blend of Sandvik and EOS powders. The green parts were processed employing commercially available equipment for the MIM process. The follow up

debinding step was performed via a solvent extraction process and afterwards the brown parts were sintered in a hydrogen atmosphere [43]. Tests were carried out on monolithic tensile bars produced with Sandvik, EOS and a blend of Sandvik and EOS powders to determine their mechanical properties (See the Appendix).

MIM test parts, i.e. the tensile bars, were afterwards cut into two halves via a 90° band saw and thus to use them as preforms for the follow up PBF operation [44]. The cut tensile bars were lightly sanded to remove any burrs. The effects of surface integrity of preforms on mechanical properties of the hybrid MIM/PBF components were investigated, too. Especially, two different surface treatments were applied on the interface surfaces of preforms, i.e. sand blasting and laser texturing [45][46]. The different conditions of MIM preform surfaces allowed the bonding strength at the interface between the MIM preforms and PBF sections to be studied.

The PBF sections of the hybrid tensile bars were built on the cut surface of the MIM preforms. In particular, the MIM preforms were placed in a PBF system, i.e. EOS M290 machine, employing custom fixtures and the modular work-holding system discussed in Section 2.1. The AM sections on top of the preforms were built by using EOS 316L stainless steel powder and the following process settings: laser power 180W; scanning speed 1300 mm/s; energy density 83 J/mm^3 and double or simple laser exposition [47] in a protective gas environment to prevent oxidation. This setup was used to manufacture hybrid 316L steel MIM/PBF tensile bars. These tensile bars were used subsequently to investigate the interfaces and mechanical performance of hybrid MIM/PBF components.

Figure 3 shows a PBF build plate with MIM preforms mounted into the custom fixture and then integrated into the PBF system to produce the hybrid tensile bars. The total number of MIM preforms required for the used 5 build plates in this research were 100 and interface surfaces on 20 of them were laser textured and another 20 were sand blasted while the interface surfaces on other 60 were used as received after the cutting operation. The slots used in the custom fixtures to fix the MIM performs with their corresponding surface treatments are provided in Table 1.

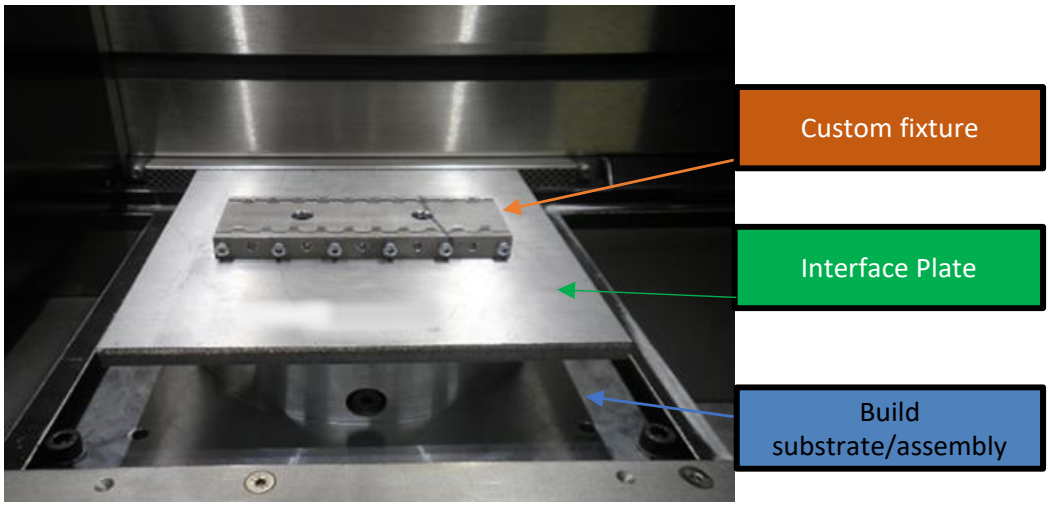

Figure 3: 20 MIM preforms mounted with a custom fixture onto a PBF build plate

Table 1: MIM performs with their corresponding surface treatments and slot IDs when fixed onto the five build plates

Plates 1-5					
MIM preform ID (slot number)	1-3	4-7	8-13	14-17	18-20
MIM preform surface condition	Sawn	Laser Textured	Sawn	Sand blasted	Sawn

2.3 Characterization of hybrid tensile bars

The following tests and characterisation work were carried out to investigate the mechanical properties of hybrid tensile bars:

- Tensile tests to measure the strength of the bonding interface between PBF sections and MIM preforms. A universal testing machine was employed. A pre-load of 3 MPa, a velocity of 6 MPa/S for the elastic region (until reaching $Rp_{0.2}$) and a constant velocity of 6 mm/min for the plastic one at ambient temperature were used in all tensile tests.
- Hardness tests were performed, too, to assess whether the welding has an impact on mechanical properties of the MIM preforms. In particular, a universal micro-hardness tester was used to assess the impact of the PBF process. Two sets of 10 Vickers indentations were carried out at 0.5- and 1-mm depth into the MIM preform and at 0.5 mm depth into the PBF section. There was 0.1 mm separation between the indentations. The load used for each indentation was 0.1 kgF with an indentation time of 10 s.
- A metallographic analysis was carried out to investigate the microstructure and the presence of any defects at the interface between the MIM preforms and PBF sections.
  SEM, EDS and Optical microscopy were used to detect defects without performing any destructive tests. In particular, SEM was employed to analyse the microstructure at the MIM/PBF interfaces and also to spot any defects. Additionally, EDS was used to analyse the chemical-elemental composition of the samples, whilst the focus variation technology was employed to investigate microstructure and weld successions at the MIM/PBF interfaces.

3. Results and Discussion

3.1 Tensile tests

The main objective of the tensile tests was to investigate the mechanical properties of the hybrid MIM/PBF components. Stress-strain properties of monolithic MIM and PBF tensile bars were analysed, first, to ensure that both preforms, and AM sections had sufficient strength and the results were used as a reference to determine the robustness of the MIM/PBF interface. Fracture surfaces and locations were also investigated.

i. Mechanical properties of monolithic PBF parts

Monolithic PBF tensile bars were produced with the EOS powder. As it was already mentioned their mechanical properties were used as a reference in investigating the performance of hybrid MIM/PBF components. PBF

specimens were produced with two different build orientations, vertical and horizontal. In addition, a positive offset of 0.3 mm was applied on the STL model to produce half of them with some machining allowance while the rest were built to net shape. Especially, the samples with 0.3 allowance were machined in order to remove any defects or residual stresses on their surfaces. In this way, the effects of the build orientation and the follow up post-processing step on mechanical properties of monolithic PBF components were investigated, too. Also, the impact of the PBF heat treatment on the mechanical properties was investigated, especially the samples were heat treated for 90 min at 900°C and then cooled down in the furnace. Prior to the tensile tests, the PBF samples were grinded and polished to remove any burrs and/or improve the surface roughness that might impair their mechanical strength.

The average results from five tensile tests carried out on the PBF specimens are presented in Figure 4, and Table 2. The red lines in the bar charts represent the requirements of the ASTM A 479 standard for 316L stainless steel [48] that were lower. Also, the results obtained with the MIM specimens, produced with the Sandvik powder, are included in Figure 4 as another reference. The following observations based on the obtained results can be made:

- As expected, the mechanical properties of the PBF tensile bars built horizontally and vertically were different. The tensile bars built vertically had a lower R_m and higher $R_{p0.2}$ and elongation at rupture compared to the tensile bars build horizontally. This results can be explained with the anisotropy of PBF parts due to the dependence of the grain structure orientation on the PBF build orientation [49] [50].

- The heat treatment had a significant impact on the elongation at rupture and $R_{p0.2}$ for the PBF specimens built horizontally. In particular, the heat treatment released the stresses in the material induced by the PBF process and therefore the elongation at rupture increased by approximately 13% while $R_{p0.2}$ was lower by approximately 15%.

- The heat treatment had a low impact on R_m and $R_{p0.2}$ for the PBF specimens build vertically compared with those built horizontally. In addition, the heat treatment has been found to reduce the elongation at rupture of the tensile bars built vertically by approximately 5%. This result can be explained with the tensile loading axis that was parallel to the build direction. Thus, the weak welded layers were parallel to cracks and this facilitated their propagation. Therefore, the vertically built samples demonstrated lower elongation than those built horizontally both as built and after the heat-treatment.

- The PBF specimens that were machined had a lower $R_{p0.2}$, higher R_m and elongation at rupture compared with the PBF tensile bars because the net shape bars exhibited more defects on the surface and therefore were more susceptible to fractures.

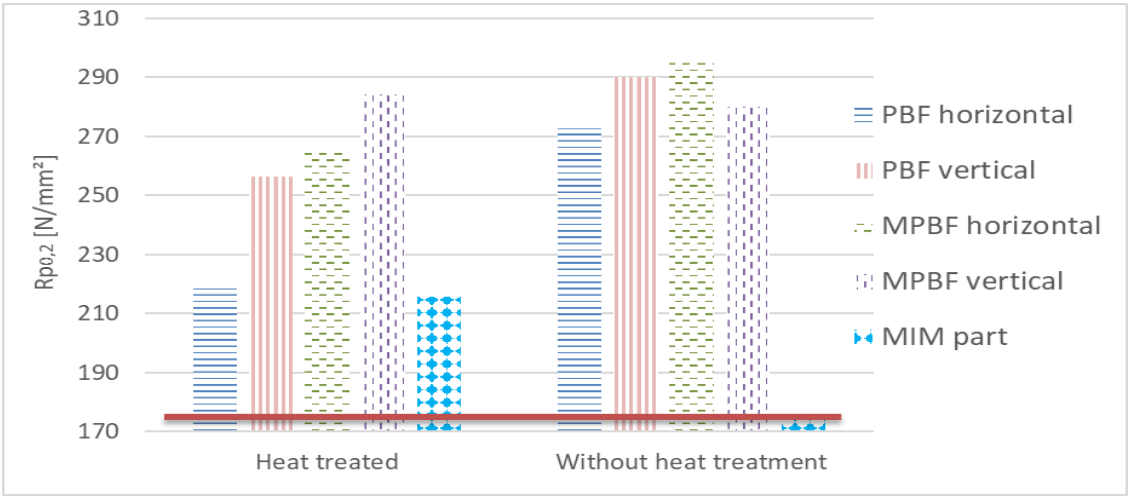

(a)

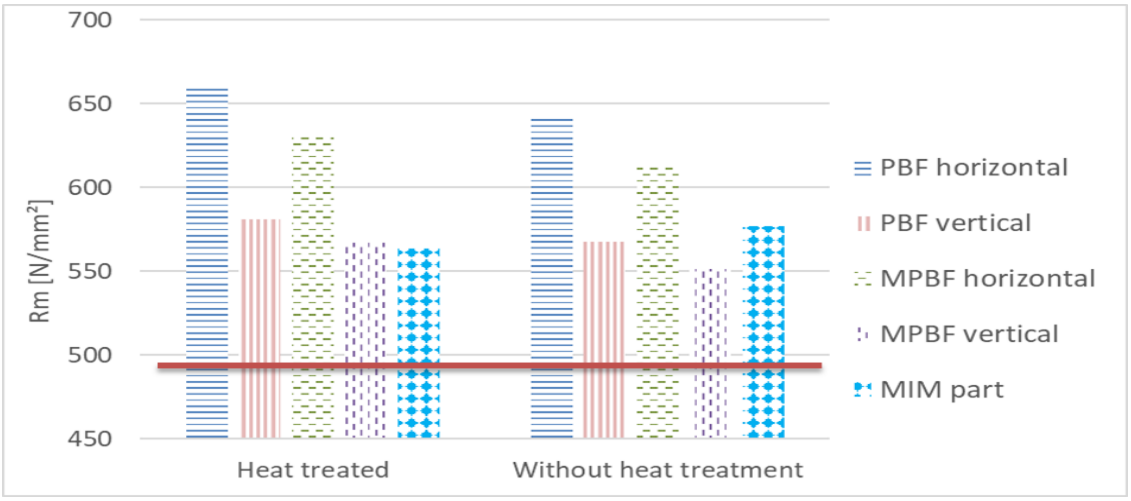

(b)

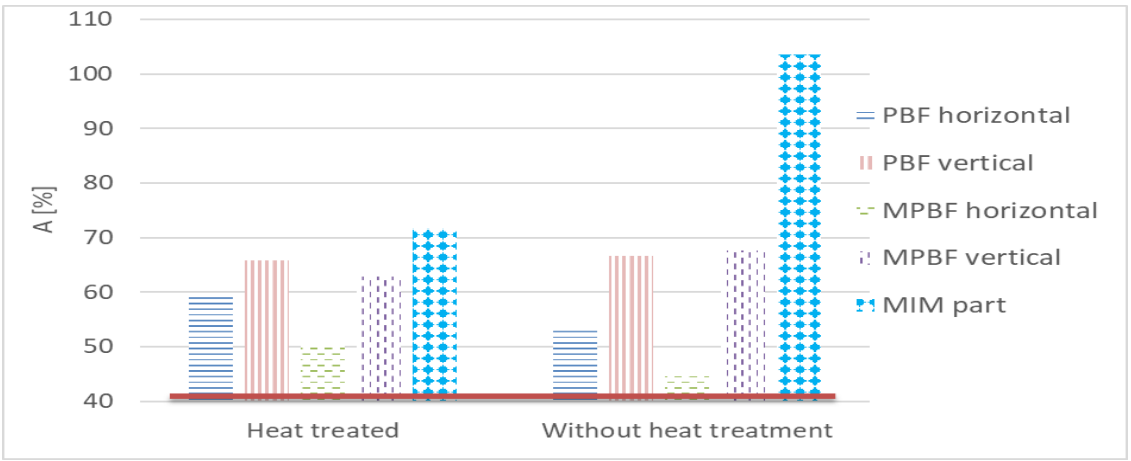

(c)

Figure 4: The mechanical properties of 316L PBF and MIM specimens: a) 0.2% offset yield strength, b) ultimate strength and c) the elongation at rupture of specimens

Note: MPBF are the specimens that were first built to near net shape and then machined to produce tensile bars

Table 2: Results of tensile tests carried out on the PBF and MIM specimens.

		Horizontal			Vertical		
		$R_{p0.2}$ [MPa]	R_m [MPa]	A [%]	$R_{p0.2}$ [MPa]	R_m [MPa]	A [%]
PBF	HT	**265,6**	**632,2**	**50,1**	**284,3**	**567,3**	**62,9**
	SD	11,2	7,4	3,1	35,9	0,6	0,4
	WHT	**296,3**	**612,3**	**44,5**	**280,2**	**551,2**	**67,7**
	SD	19,5	9,2	2,2	21,3	3,3	3,0
PBF+Machined	HT	**218,3**	**661,3**	**59,7**	**256,4**	**581,2**	**65,8**
	SD	18,3	3,1	2,2	20,1	8,1	3,3
	WHT	**272,6**	**643,2**	**53,0**	**290,3**	**567,5**	**66,7**
	SD	38,7	4,0	2,1	49,0	3,9	8,6
Sandvik MIM	HT	216	539	72			
	SD	9	1	1			
	WHT	175	577	104			
316L Standard ASTM A 420		172	485	40			

Note: HT denote the specimens with the PBF heat treatment; SD – the standard deviation of five measurements; WHT – the specimens that did not undergo the heat treatment.

Compared to the properties of the 316L MIM specimens, the PBF ones had a higher $R_{p0.2}$ and a lower elongation. The resulting residual stresses are dependent on the build orientation and therefore R_m of the PBF specimens built horizontally is higher than that of the MIM bars while R_m of the PBF bars built vertically was similar or marginally lower. Also, it should be noted that PBF specimens with and without heat treatment had a higher standard deviation for the yield stress and this was attributed to their high residual stresses.

ii. Mechanical properties of hybrid MIM/PBF components

The quality and reproducibility of hybrid MIM/PBF components were investigated, especially their interface performance. A design of experiments (DOE) was carried out with three controlled factors, i.e. MIM surface treatment (Sawn, Laser textured, Sand blasted), PBF heat treatment (with and without) and PBF laser exposition (simple or double).

The system level tools together with the specially designed custom fixtures described in Section 2.1 were used to produce 100 hybrid tensile bars, especially five batches of twenty were built to assess the reproducibility of the used multi-setup HM approach. The same procedure and process settings were used for all batches while the DOE factors were varied. In particular, the preparation of the interface surfaces on MIM preforms was varied to investigate the effects of laser exposition and heat treatment on mechanical properties**.** The values of the controlled factors used for each sample in the five PBF builds are provided in Table 3.

Especially, two surface treatments, i.e. laser texturing and sand blasting, were applied to determine whether such pre-processing might have an impact on the bonding strength of the interfaces and the sample's mechanical properties. Four samples were laser textured and sand blasted while the other 12 in each batch were used as received (sawn). As discussed in section 3.1, the PBF samples that did not undergo heat treatment demonstrated a higher SD compared to the heat-treated ones and thus led to lower Rm due to high residual stresses. Therefore, the heat treatment was essential in achieving the required stress relief and as such it was applied on most samples, i.e. 18 samples in each batch. The other two samples in each batch were used as a reference in evaluating the impact of the heat treatment on the mechanical performance and microstructure of hybrid samples. In addition,

two laser exposition setting in the PBF process, i.e. the double and simple laser exposition, were applied to study if they had any effect on samples' mechanical behaviour. Only three samples per batch were produced with the double exposition as such settings would affect the PBF processing time. Finally, surface preparation (laser texturing and sand blasting) and double laser exposition were not applied simultaneously on samples in order to study their potential effects independently. Multiple samples were produced with each process setting to investigate the process repeatability in regards, to the mechanical properties. Especially, the performance of MIM/PBF interfaces.

Table 3: The values of the controlled factors used to build 20 tensile bars in each of the 5 PBF builds

MIM Preform ID	1	2	3	4	5	6	7	8	9	10	11	12	13	14	15	16	17	18	19	20
MIM Surface treatment	Sawn	Sawn	Sawn	Laser Textured	Laser Textured	Laser Textured	Laser Textured	Sawn	Sawn	Sawn	Sawn	Sawn	Sawn	Sand Blasted	Sand Blasted	Sand Blasted	Sand Blasted	Sawn	Sawn	Sawn
Heat treatment	Yes	Yes	Yes	Yes	Yes	Yes	Yes	Yes	Yes	No	Yes	Yes	Yes	Yes	Yes	Yes	Yes	Yes	No	Yes
PBF Exposition	Double	Double	Double	Simple	Simple	Simple	Simple	Simple	Simple	Simple	Simple	Simple	Simple	Simple	Simple	Simple	Simple	Simple	Simple	Simple

The tensile bars in each of the 5; PBF builds were numbered with the preform's IDs as shown in Table 3. In particular, tensile tests were conducted on 13 samples, i.e. 1-2, 4-5, 8-13, 15-16 and 18, specimens, while the others were used to study hardness and microstructure at the MIM/PBF interfaces employing SEM and optical microscopy, especially to identify the presence of any defects at the interfaces.

The fracture in tensile bars was expected to be in the PBF sections due to their vertical orientation in the builds, particularly due to higher R_m of the MIM preforms. 65 tensile tests were carried out and from them only 36 presented a ductile facture in the PBF sections as expected. Representative specimens, i.e. sample 5-12, with a ductile fracture are shown in Figure 5(a-b), where the rupture occurred as a result of the progressive reduction of the PBF cross section. The characteristic surface of a ductile fracture with a wall of cup and cone topography is depicted in Figure 5(c-d).

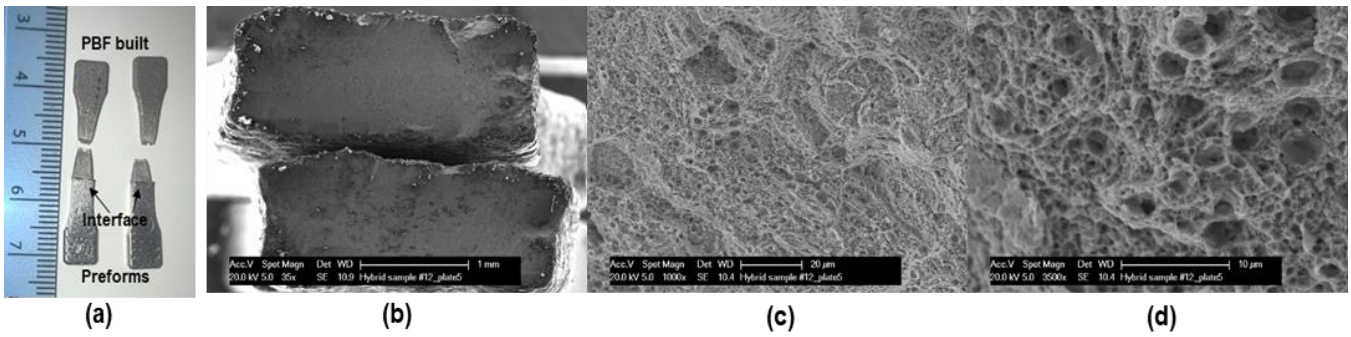

Figure 5: (a) Image of fractured samples, SEM fractography of ductile fracture surfaces in the PBF section of a sample: (b) shrunk cross section, (c) a ductile fracture with a dimpled topography, (d) a wall of cup and cone topography.

The rest of the tensile tests, i.e. 27 from the total number of 65, exhibited a brittle fracture within the MIM preforms near the interfaces. A representative example is provided in Figure 6(a) where no reduction of the bar cross section can be observed, whilst the characteristic surface for an intergranular fracture can be seen in the fractography Figure 6(b-c).

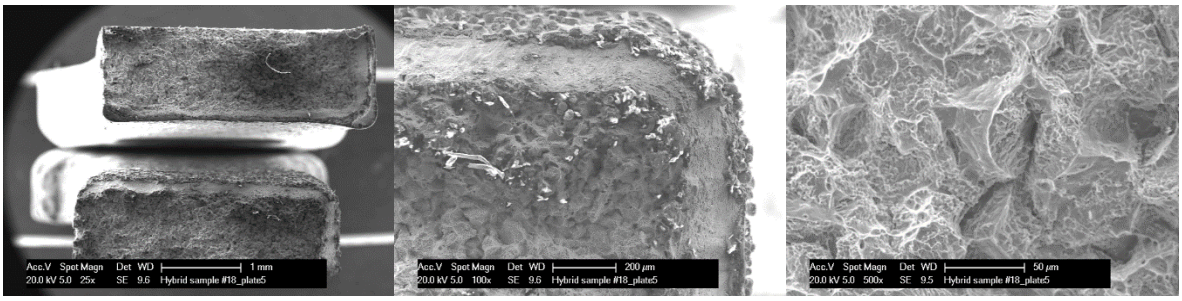

(a) **(b)** **(c)**

Figure 6: SEM fractography of the brittle fracture surface of a sample. (a) non-shrunk cross section, (b) intergranular cross section, (c) intergranular topography.

The different modes of failure observed in the carried out 65 tests were analysed with the Minitab software to explain the reasons for the different results. In particular, the impact of investigated controlled factors, i.e. surface texturing, heat treatment, PBF laser exposition, on mechanical properties, i.e. Rm, Rp0.2 and elongation at rupture, and also on the fracture mode were analysed.

The results of these analysis are provided in Figure 7(a), 8(a) and 9(a). It shows that despite the fact that all 5 batches of hybrid tensile bars were produced with the same process settings, there were substantial differences between the mechanical properties across the five batches. For example, the mechanical properties increased progressively from batch one to five and the best values were obtained in batch five. These results can explain the reduction of brittle fracture near the interface from batches one to five, in particular, the brittle fractures of 1st, 2nd, 7th, 8th and 9th specimens in batches one to five, respectively. At the same time, the mechanical properties of the tensile bars with a brittle facture were lower than those of the samples with ductile fracture as shown in Table 4. Therefore, if the tensile bars with brittle fractures are excluded and only the results from the samples with ductile fractures are analysed (see Figure 7(b), 8(b) and 9(b)) the following observations can be made:

- The ductility of hybrid specimens is practically the same across the five batches (66% with a deviation of +/-5%).
- All the hybrid specimens produced in batches one and two have a lower R_m and $R_{p0.2}$ than those built in batches three to five. This could be explained by some cross contamination in batches one and two from previous builds in the PBF system.
- The heat treatment had the same impact on the hybrid specimens as on the monolithic PBF samples, namely an increase of $R_{p0.2}$ and R_m and a marginal decrease of ductility.
- The surface preparation on the MIM preforms did not have noticeable effects on mechanical properties and on the fracture mode. This is mainly attributed to the melt pool and heat affected zone created in the PBF process, which penetrates at least a few hundred microns below into the subsurface of the substrate and in this way eliminates the effects of any prior surface preparation. The PBF processing conditions

and their overall impact are directly related to the used laser processing settings, i.e. laser power, material absorption coefficient, etc. [51][52].

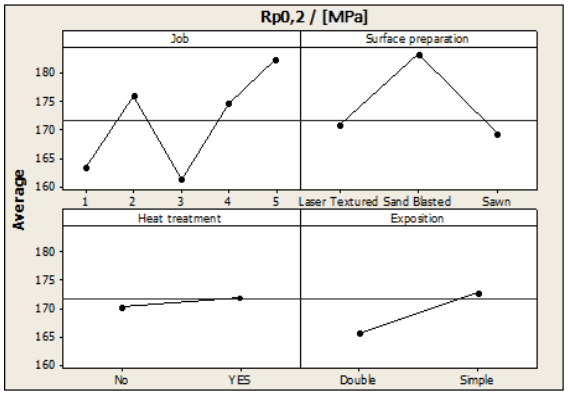

(a) All tensile tests

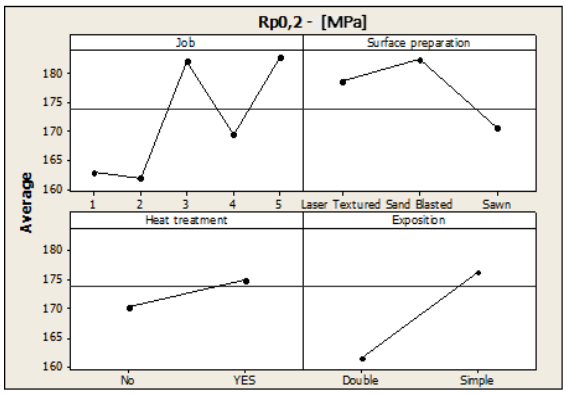

(b) Only samples with ductile fracture in PBF sections

Figure 7: The analysis of controlled factors' effects on Rp0.2.

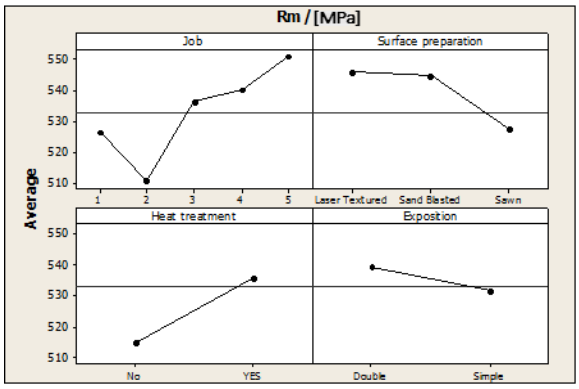

(a) All tensile tests

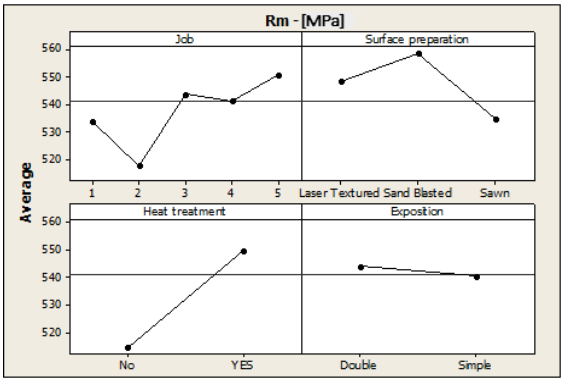

(b) Only samples with ductile fracture in PBF sections

Figure 8: The analysis of controlled factors' effects on R_m.

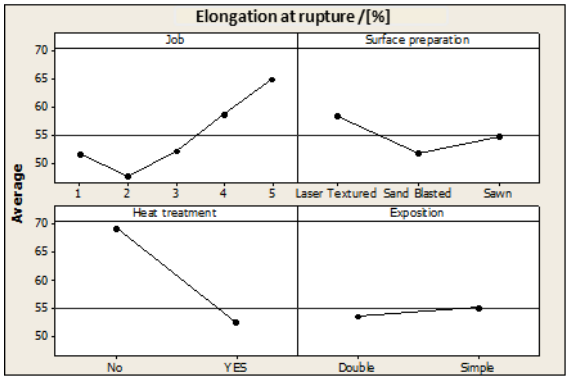

(a) All tensile tests

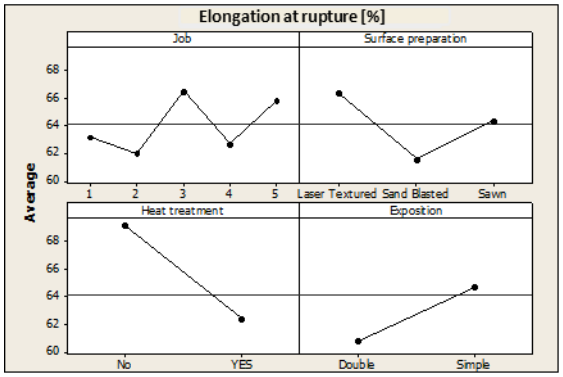

(b) Only sample with ductile fracture in PBF sections

Figure 9: The analysis of controlled factors' effects on elongation at rupture.

Table 4: Mechanical properties of hybrid specimens with ductile and brittle fractures.

		Hybrid specimens with ductile fracture			Hybrid specimen with brittle fracture		
		$R_{p0.2}$ [MPa]	R_m [MPa]	A [%]	$R_{p0.2}$ [MPa]	R_m [MPa]	A [%]
Heat treated	Average	**175,7**	**549,7**	**62,4**	**169,0**	**522,1**	**43,6**
	SD	25,1	13,2	7,2	27,0	31,8	11,2
Without heat treatment	Average	**170,3**	**514,9**	**69,2**	**No brittle fracture**		
	SD	19,5	10,5	1,3			

The varying fracture modes of the hybrid samples can be attributed to two factors:

1. All tensile bars without heat treatment had a ductile fracture in the PBF section. The heat treatment had an impact on the ductility of the MIM parts, especially there was a precipitation of a brittle phase at the grain boundaries. Therefore, one of the factors that affected the fracture mode can be the thermal load induced by the laser melting of initial PBF layers that can increase this embrittlement effect and thus to lead to brittle fractures into the MIM preforms close to the interface. However, this is just a hypothesis and it is not sufficient to explain the big reduction of brittle fractures from nine specimens in batch two to just one in batch five.
2. Some misalignment between the MIM preforms and the PBF sections could be another reason for the different fracture modes across the specimens. In particular, any misalignment creates a step between the MIM preform and the PBF section as depicted in Figure 10. In particular, the build region has an offset of a few hundreds of microns from the boundaries of the MIM preform and thus shows a virgin without a PBF built flat area close to the surface edges. During the tensile tests, any misalignment can potentially induce a stress concentration at the interface, and this combined with the decrease of the MIM ductility can result in a brittle fracture.

These two factors explain to some extent the brittle fracture phenomenon, but they are not conclusive, and further analysis is required.

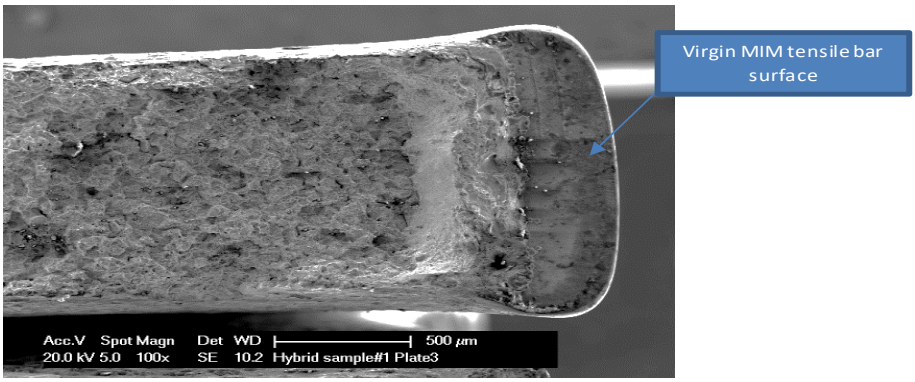

Figure 10: A SEM fractography of a brittle fracture surface and misalignment on a MIM preform.

3.2 Characterization of MIM/PBF interfaces

Five hybrid tensile bars, i.e. samples three, six, 17,19 and 20, from each of the five batches were used for characterising MIM/PBF interfaces, i.e. for metallographic, hardness and chemical composition analyses, and thus to investigate whether the surface treatments of the MIM preforms and the heat treatment had an impact on interface morphology.

i. Metallographic analysis of MIM/PBF interfaces

A SEM analysis of MIM/PBF interfaces after their etching were performed. Each hybrid tensile bar was encapsulated in resin and polished to perform this analysis.

SEM micrographs were taken from the prepared specimens to determine whether voids or cracks were present at MIM/PBF interfaces. The micrographs showed that the MIM/PBF interfaces of all samples irrespective of surface and heat treatments and processing conditions were crack-void free. Figure 11 shows a representative micrograph of one analysed interface.

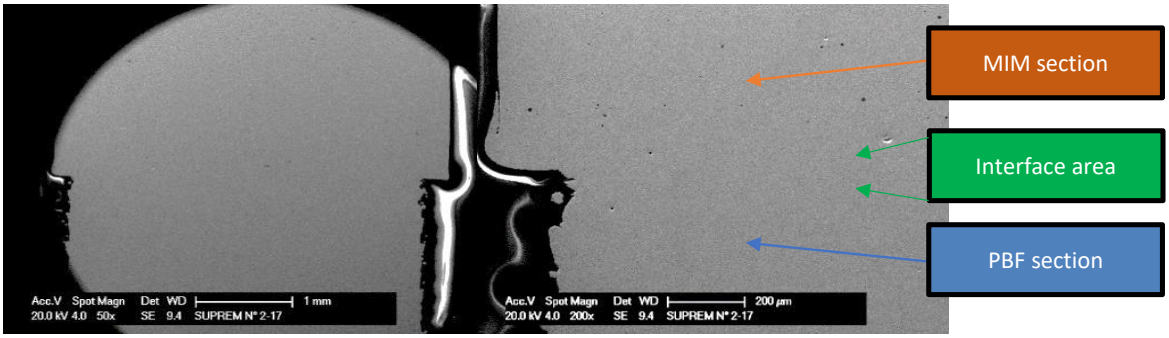

Figure 11: A SEM micrograph of a MIM/PBF interface.

Then, the prepared specimens were etched to analyze the microstructure at the MIM/PBF interface. An electro-etching with oxalic acid as electrolyte was applied to reveal the microstructure. A representative image that depicts the microstructure obtained on hybrid samples with and without heat treatment are presented in Figure 12 and 13, respectively.

The analysis of the optical micrographs confirmed again that the MIM/PBF interfaces were free from any voids or cracks and so was considered "healthy", without any defects. The microstructures of the MIM and PBF sides of the interface were as expected different, i.e. with regular grains and a succession of welds on the MIM and PBF sides, respectively. The samples that did not underwent heat treatment (see Figure 13), the interface between the MIM preforms and the PBF sections were well defined, whereas there were superposition characteristics of two different microstructures with grains around 100 µm after the heat treatment (see Figure 12). The weld areas start to turn into a conventional 316L microstructure with regular grains after 100 µm from the interface, both on samples with and without heat treatment.

The two images show also that one/two layers of grains into the MIM preforms are re-melted or welded during the PBF process and this could have an impact on mechanical properties. This welding of MIM preforms was investigated by performing hardness tests and thus to determine what is the effect on the interface. The results are presented in the following section.

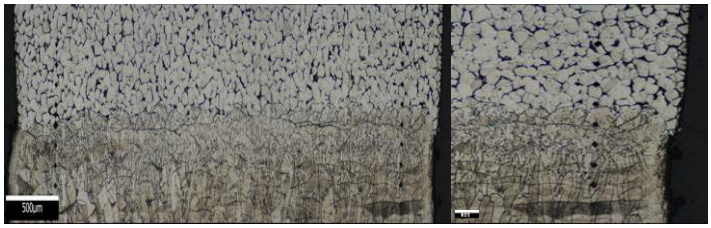

Figure 12: An image of the MIM/PBF interface after heat treatment by electro etching of specimen 1-3.

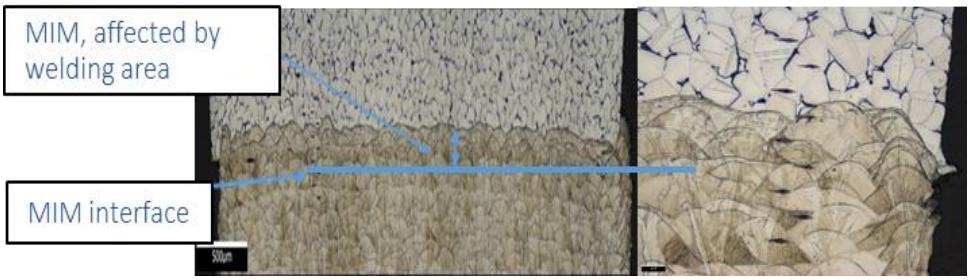

Figure 13: An image of the MIM/PBF interface without heat treatment after electro etching of specimen 1-19.

A further EDS analysis was carried out to study the chemical composition of the samples and also to investigate the black phases at the grains' boundaries. The images show clearly a black phase precipitation around the grains that suggest a presence of intermetallic phases [53]. These phases are found to mainly contain a high percentage of carbon, potassium and other elements. The comparison with the ASTM B883 standard shows that the obtained results deviate from the standard regarding the chemical composition of the hybrid samples.

Therefore, the samples were analysed further after mechanically polishing them to reveal the subsurface of the interface on the MIM side and thus not to be confined superficially just to the surface. Surprisingly, the repeated

EDS analysis had shown that there were intermetallic free areas in the subsurface layers and also the chemical composition complied with the ASTM standards. Tables 5 and 6 provide information about the respective chemical compositions before and after the mechanical polishing, respectively. Thus, the results revealed that the elements found prior to the mechanical polishing were mainly contaminations from different powders used in the PBF chamber before the five batches of hybrid tensile bars were produced. In addition, holes were induced after the etching that dissolved the ferrite and or sigma phases. Moreover, the heat treatment introduced some further contamination that subsequently adhered to the surface of the samples but was removed after the mechanical polishing.

Table 5: Black spot Spectrum calculation prior to the mechanical polishing

Element	Series	Mass C. [wt.%]	norm. C. [wt.%]	Atom C. [at.%]	Error (3 Sigma) [wt.%]
C	K series	28,94	54,78	77,84	11,39
Mn	K series	0,24	0,45	0,14	0,13
Si	K series	0,01	0,02	0,01	0,08
Cr	K series	0,83	1,56	0,51	0,18
Ni	K series	0,94	1,78	0,52	0,23
Mo	L series	0,67	1,27	0,23	0,16
P	K series	0,00	0,00	0,00	
S	K series	0,82	1,56	0,83	0,17
N	K series	1,69	3,19	3,89	1,63
Fe	K series	3,47	6,57	2,01	0,44
Na	K series	1,44	2,72	2,02	0,36
Cl	K series	7,16	13,55	6,52	0,80
K	K series	6,63	12,55	5,48	0,70
	Total	**52,82**	**100,00**	**100,00**	

Table 6: Black spot Spectrum calculations after the polishing

Element	Series	Mass C. [wt.%]	norm. C. [wt.%]	Atom C. [at.%]	Error (3 Sigma) [wt.%]
C	K series	1,30	1,09	4,79	0,89
K	K series	0,12	0,10	0,14	0,09
Ca	K series	0,18	0,15	0,20	0,10
Ti	K series	0,26	0,22	0,24	0,11
Cr	K series	18,99	15,91	16,19	1,73
Mn	K series	0,96	0,80	0,77	0,18
Fe	K series	82,95	69,50	65,84	7,37
Ni	K series	13,38	11,21	10,11	1,36
Al	K series	0,00	0,00	0,01	0,08
Si	K series	0,26	0,22	0,41	0,12
P	K series	0,06	0,05	0,08	0,09
S	K series	0,83	0,70	1,15	0,17
Cl	K series	0,07	0,06	0,09	0,09
	Total	**119,36**	**100,00**	**100,00**	

ii. Hardness analysis

Hardness tests were conducted to determine whether the PBF process modified somehow the mechanical properties at/or near the MIM/PBF interface. In particular, micro hardness tests were performed that included a succession of ten Vickers indentations at 1 and 0.5 mm from the interfaces into the MIM preforms and 0.5 mm into the PBF sections. There was a separation of 0.1 mm between the indentations while the load applied was 0.1 kgF for 10 s. Figure 14 depicts the two lines of indentation into the MIM preform of hybrid sample 5-3.

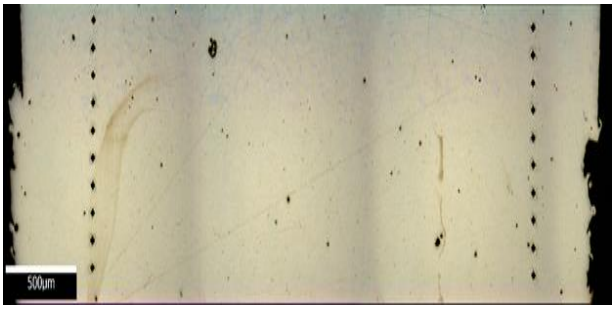

Figure 14: An image of sample 5-3 with the two lines of Vickers indentations into the preform.

The graph in Figure 15 presents representative results obtained from the hybrid samples produced in batch five, i.e. 5-3, 5-6, and 5-17 samples. These results show that as expected the hardness of MIM preforms was lower

than that of the PBF sections. However, the PBF process induced a gradual hardening of the MIM preform closer to the interface. In addition, a gradual increase of hardness from the MIM preform towards the PBF sections can be clearly seen in the figure.

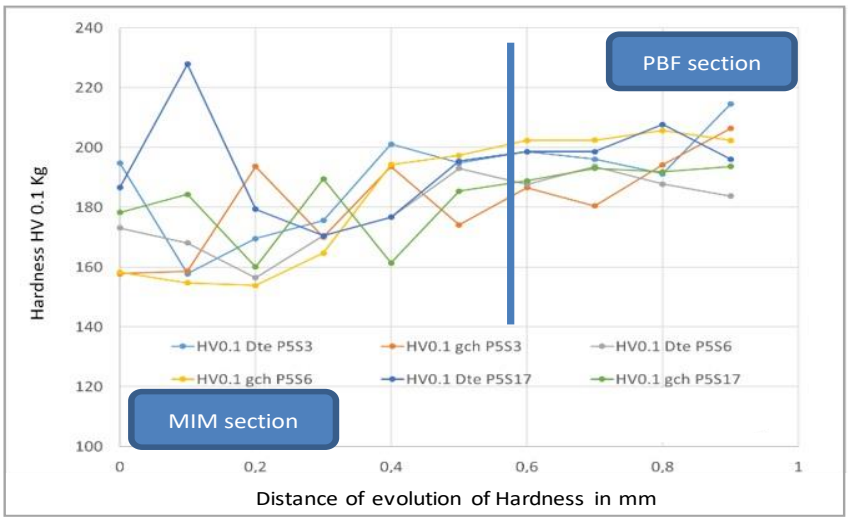

Figure 15: The evolution of the hardness between the MIM preform and the PBF section of the samples produced in batch five, the blue bar depicts the interface area.

Table 7 presents the average results of microhardness tests performed on Specimens three, six, 17 and 19 produced in each of the five batches with two investigated surfaces and heat treatments. The results show that the different surface treatments on the MIM preforms did not affect the hardness results. At the same time, the heat treatment of the hybrid samples led to a reduction of the hardness results for the PBF sections while the hardness of the MIM preforms was not affected.

Table 7: Average results of micro hardness measurements for the hybrid samples in 5 batches

	Treatments	MIM	PBF	MIM SD	PBF SD
Sample 3	HT + Sawn	177	198	18	10
Sample 6	HT + Laser Texturing	177	194	22	8
Sample 17	HT + Sand Blasting	175	203	16	10
Sample 19	WHT + Sawn	177	223	21	2

Notes: HT – with heat treatment; WHT – without heat treatment; Sawn, Laser Texturing and Sand Blasting – the surface treatment of MIM preforms; SD – standard deviation.

4. Conclusions

The mechanical properties and interfaces of all hybrid components produced employing a multi-setup HM approach, i.e. combining the capabilities of MIM and PBF processes, were investigated in this research. The obtained results show that the proposed HM route can produce hybrid MIM/PBF components with consistent mechanical properties and interface performance. In particular, the following conclusions can be made based on the obtained results:

- The material properties and the performance of interfaces between MIM preforms and PBF sections were similar and even better than the properties of monolithic MIM parts. While they conformed fully to the ASTM standards for 316L stainless steel parts.

- The investigated treatments of the MIM interface surfaces, i.e. laser texturing, sandblasting and as received after the sawing, did not have any impact on the interface performance and also on the fracture mode.

- Any misalignment between the MIM preform and PBF sections can potentially induce stress concentrations at the interface and thus to initiate the crack propagation that in combination with the decrease of MIM ductility can result in a brittle fracture. Thus, the use of modular workpiece holding devices with custom fixtures that can minimise any misalignments is crucial in producing hybrid components with required MIM/PBF interface performance.

- The heat treatment of hybrid MIM/PBF components affects the fracture mechanism. As all hybrid specimens without heat treatment had a ductile fracture in the PBF section, whilst for heat treated ones exhibited a brittle fracture within the MIM preforms near the interfaces. However, it is important to note that the brittle fracture decreased progressively with the improvement of mechanical properties from batch 1 to 5 and this can be attributed to a precipitation of brittle phases at the grain boundaries of the MIM preforms.

- The thermal load induced by the laser melting during the initial PBF layers can increase the embrittlement effect and thus can lead to brittle fractures into the MIM preforms close to the interface. However, it should be noted that this effect on MIM performs of hybrid components cannot explain fully the big reduction of brittle fractures from the first two to the last three PBF batches and further research is required.

The microstructure analysis of MIM/PBF interfaces reviled that they were free from any voids or cracks and thus could be considered “healthy”, without any defects. Thus, the interface cross sections did not show any sign of cracks or void which would clearly explain and justify the reasons why fractures occurred at the interface area. A further analysis showed precipitation of black phases around the grains closer to the interfaces that suggest a presence of intermetallic phases. However, they were removed after mechanical polishing and therefore were considered mainly contaminations from different powders used in the PBF chamber before the hybrid components were produced.

5 References

[1] "PLM−Product Lifecycle Management: Siemens PLM Software." [Online]. Available: https://www.plm.automation.siemens.com/global/en/. [Accessed: 20-Sep-2018].

[2] A.-K. Reichler *et al.*, "Incremental Manufacturing: Model-based part design and process planning for Hybrid Manufacturing of multi-material parts," *Procedia CIRP*, vol. 79, pp. 107–112, 2019, doi: 10.1016/j.procir.2019.02.020.

[3] J.-H. Schmitt and T. Iung, "New developments of advanced high-strength steels for automotive applications," *Comptes Rendus Phys.*, vol. 19, no. 8, pp. 641–656, Dec. 2018, doi: 10.1016/J.CRHY.2018.11.004.

[4] C. CHEN, Y. ZHENG, Y. ZHANG, X. LU, and C. SHANG, "Life Prediction of Newly Developed Ferritic Stainless Steels for Automotive Muffler," *J. Iron Steel Res. Int.*, vol. 21, no. 1, pp. 125–130, Jan. 2014, doi: 10.1016/S1006-706X(14)60020-0.

[5] European Commission, *Factories of the Future Ppp Strategic Multi-Annual Roadmap*. 2010.

[6] B. Lauwers, F. Klocke, A. Klink, A. E. Tekkaya, R. Neugebauer, and D. Mcintosh, "Hybrid processes in manufacturing," *CIRP Ann.*, vol. 63, no. 2, pp. 561–583, Jan. 2014, doi: 10.1016/J.CIRP.2014.05.003.

[7] S. T. Newman, Z. Zhu, V. Dhokia, and A. Shokrani, "Process planning for additive and subtractive manufacturing technologies," *CIRP Ann.*, vol. 64, no. 1, pp. 467–470, 2015, doi: 10.1016/j.cirp.2015.04.109.

[8] T. Bakša, T. Kroupa, P. Hanzl, and M. Zetek, "Durability of Cutting Tools during Machining of Very Hard and Solid Materials," *Procedia Eng.*, vol. 100, pp. 1414–1423, Jan. 2015, doi: 10.1016/J.PROENG.2015.01.511.

[9] D. Ulutan and T. Ozel, "Machining induced surface integrity in titanium and nickel alloys: A review," *Int. J. Mach. Tools Manuf.*, vol. 51, no. 3, pp. 250–280, Mar. 2011, doi: 10.1016/j.ijmachtools.2010.11.003.

[10] D. A. Axinte, P. Andrews, W. Li, N. Gindy, P. J. Withers, and T. H. C. Childs, "Turning of advanced Ni based alloys obtained via powder metallurgy route," *CIRP Ann.*, vol. 55, no. 1, pp. 117–120, Jan. 2006, doi: 10.1016/S0007-8506(07)60379-5.

[11] R. Dubovska, J. Jambor, and J. Majerik, "Implementation of CAD/CAM System CATIA V5 in Simulation of CNC Machining Process," *Procedia Eng.*, vol. 69, pp. 638–645, Jan. 2014, doi: 10.1016/J.PROENG.2014.03.037.

[12] C. Qiu, N. J. E. Adkins, H. Hassanin, M. M. Attallah, and K. Essa, "In-situ shelling via selective laser melting: Modelling and microstructural characterisation," *Mater. Des.*, vol. 87, pp. 845–853, Dec. 2015, doi: 10.1016/j.matdes.2015.08.091.

[13] P. K. Gokuldoss, S. Kolla, and J. Eckert, "Additive Manufacturing Processes: Selective Laser

Melting, Electron Beam Melting and Binder Jetting-Selection Guidelines.," *Mater. (Basel, Switzerland)*, vol. 10, no. 6, Jun. 2017, doi: 10.3390/ma10060672.

[14] D. Herzog, V. Seyda, E. Wycisk, and C. Emmelmann, "Additive manufacturing of metals," *Acta Mater.*, vol. 117, pp. 371–392, Sep. 2016, doi: 10.1016/J.ACTAMAT.2016.07.019.

[15] P. Penchev *et al.*, "System-level integration tools for laser-based powder bed fusion enabled process chains," *J. Manuf. Syst.*, vol. 50, pp. 87–102, Jan. 2019, doi: 10.1016/J.JMSY.2018.12.003.

[16] H. Hassanin, A. A. Al-Kinani, A. Elshaer, E. Polycarpou, M. A. El-Sayed, and K. Essa, "Stainless steel with tailored porosity using canister-free hot isostatic pressing for improved osseointegration implants," *J. Mater. Chem. B*, vol. 5, no. 47, pp. 9384–9394, 2017, doi: 10.1039/c7tb02444d.

[17] D. Bhaduri *et al.*, "Laser polishing of 3D printed mesoscale components," *Appl. Surf. Sci.*, vol. 405, pp. 29–46, May 2017, doi: 10.1016/J.APSUSC.2017.01.211.

[18] Z. Quan *et al.*, "Additive manufacturing of multi-directional preforms for composites: opportunities and challenges," *Mater. Today*, vol. 18, no. 9, pp. 503–512, Nov. 2015, doi: 10.1016/J.MATTOD.2015.05.001.

[19] W. E. Frazier, "Metal Additive Manufacturing: A Review," *J. Mater. Eng. Perform.*, vol. 23, no. 6, pp. 1917–1928, Jun. 2014, doi: 10.1007/s11665-014-0958-z.

[20] K. Essa, P. Jamshidi, J. Zou, M. M. Attallah, and H. Hassanin, "Porosity control in 316L stainless steel using cold and hot isostatic pressing," *Mater. Des.*, vol. 138, pp. 21–29, Jan. 2018, doi: 10.1016/j.matdes.2017.10.025.

[21] S. Gorsse, C. Hutchinson, M. Gouné, and R. Banerjee, "Additive manufacturing of metals: a brief review of the characteristic microstructures and properties of steels, Ti-6Al-4V and high-entropy alloys.," *Sci. Technol. Adv. Mater.*, vol. 18, no. 1, pp. 584–610, 2017, doi: 10.1080/14686996.2017.1361305.

[22] T. Ebel, "Titanium MIM for manufacturing of medical implants and devices," *Titan. Med. Dent. Appl.*, pp. 531–551, Jan. 2018, doi: 10.1016/B978-0-12-812456-7.00024-X.

[23] R. M. German and S. K. Ferchalk, "Metal and Ceramic Injection Molding — Technical Status and Future Challenges," *Most*, no. August, pp. 30–40, 2015.

[24] V. Friederici and T. Hartwig, "Metal Injection Moulding of Titanium Medical Components," *Key Eng. Mater.*, vol. 704, pp. 155–160, Aug. 2016, doi: 10.4028/www.scientific.net/KEM.704.155.

[25] "MIM-Expert Group Powder Injection Moulding Metal Injection Moulding (MIM)."

[26] G. Schlieper, "Tooling for metal injection molding (MIM)," *Handb. Met. Inject. Molding*, no. Mim, pp. 93–108, 2012, doi: 10.1533/9780857096234.1.93.

[27] K. Essa *et al.*, "Manufacturing of metallic micro-components using hybrid soft lithography and micro-electrical discharge machining," *Int. J. Adv. Manuf. Technol.*, vol. 91, no. 1–4, pp. 445–452, Jul. 2017, doi: 10.1007/s00170-016-9655-4.

[28] H. Hassanin, K. Essa, C. Qiu, A. M. Abdelhafeez, N. J. E. Adkins, and M. M. Attallah, "Net-shape manufacturing using hybrid selective laser melting/hot isostatic pressing," *Rapid Prototyp.*

J., vol. 23, no. 4, pp. 720–726, 2017, doi: 10.1108/RPJ-02-2016-0019.

[29] H. R. The World's First Hybrid Turbine Blade & Turbo Fan Remanufacturing Machine, "Hamuel Maschinenbau- HSTM - Hybrid manufacturing," 2013. [Online]. Available: https://www.hamuel.de/en/produkte/hstm/hybrid/index.php. [Accessed: 07-Dec-2018].

[30] "LASERTEC 65 3D hybrid - ADDITIVE MANUFACTURING Machines by DMG MORI." [Online]. Available: https://uk.dmgmori.com/products/machines/advanced-technology/additive-manufacturing/powder-nozzle/lasertec-65-3d-hybrid. [Accessed: 07-Dec-2018].

[31] J. M. Flynn, A. Shokrani, S. T. Newman, and V. Dhokia, "Hybrid additive and subtractive machine tools – Research and industrial developments," *Int. J. Mach. Tools Manuf.*, vol. 101, pp. 79–101, Feb. 2016, doi: 10.1016/J.IJMACHTOOLS.2015.11.007.

[32] P. Penchev, S. Dimov, D. Bhaduri, and S. L. Soo, "Generic integration tools for reconfigurable laser micromachining systems," *J. Manuf. Syst.*, vol. 38, pp. 27–45, Jan. 2016, doi: 10.1016/J.JMSY.2015.10.006.

[33] K. Boivie[1], K. Sørby[2], V. Brøtan[2], and P. Ystgaard[1], "DEVELOPMENT OF A HYBRID MANUFACTURING CELL; Integration of Additive Manufacturing with CNC Machining."

[34] D. Bhaduri *et al.*, "Evaluation of surface/interface quality, microstructure and mechanical properties of hybrid additive-subtractive aluminium parts," *CIRP Ann.*, vol. 68, no. 1, pp. 237–240, Jan. 2019, doi: 10.1016/j.cirp.2019.04.116.

[35] B. Graf, A. Gumenyuk, and M. Rethmeier, "Laser metal deposition as repair technology for stainless steel and titanium alloys," *Phys. Procedia*, vol. 39, pp. 376–381, 2012, doi: 10.1016/j.phpro.2012.10.051.

[36] J. B. Jones, P. McNutt, R. Tosi, C. Perry, and D. I. Wimpenny, "Remanufacture of turbine blades by laser cladding, machining and in-process scanning in a single machine," 2012.

[37] M. Praniewicz, T. Kurfess, and C. Saldana, "Adaptive geometry transformation and repair for hybrid manufacturing," *Procedia Manuf.*, vol. 26, pp. 228–236, Jan. 2018, doi: 10.1016/J.PROMFG.2018.07.031.

[38] S. Yin *et al.*, "Hybrid additive manufacture of 316L stainless steel with cold spray and selective laser melting: Microstructure and mechanical properties," *J. Mater. Process. Technol.*, vol. 273, p. 116248, Nov. 2019, doi: 10.1016/J.JMATPROTEC.2019.05.029.

[39] D. B. Kim, P. Witherell, R. Lipman, and S. C. Feng, "Streamlining the additive manufacturing digital spectrum: A systems approach," *Addit. Manuf.*, vol. 5, pp. 20–30, Jan. 2015, doi: 10.1016/J.ADDMA.2014.10.004.

[40] M. Merklein, D. Junker, A. Schaub, and F. Neubauer, "Hybrid Additive Manufacturing Technologies – An Analysis Regarding Potentials and Applications," *Phys. Procedia*, vol. 83, pp. 549–559, Jan. 2016, doi: 10.1016/J.PHPRO.2016.08.057.

[41] N. Gardan and A. Schneider, "Topological optimization of internal patterns and support in additive manufacturing," *J. Manuf. Syst.*, vol. 37, pp. 417–425, Oct. 2015, doi: 10.1016/J.JMSY.2014.07.003.

[42] "MIMplus technologies GmbH & Co. KG | Deutschland." [Online]. Available: https://www.mimplus.com/. [Accessed: 12-Apr-2019].

[43] M. Zhao *et al.*, “Investigation of the solvent debinding in the injection molding of ZrO2 ceramics using LDEP, HDPE and wax binders,” *Ceram. Int.*, vol. 45, no. 3, pp. 3894–3901, Feb. 2019, doi: 10.1016/J.CERAMINT.2018.11.062.

[44] D. Albrecht and H.-C. Möhring, “Potentials for the optimization of sawing processes using the example of bandsawing machines,” *Procedia Manuf.*, vol. 21, pp. 567–574, Jan. 2018, doi: 10.1016/J.PROMFG.2018.02.157.

[45] B. Miao, L. Song, Y. Chai, K. Wei, and J. Hu, “The effect of sand blasting pretreatment on plasma nitriding,” *Vacuum*, vol. 136, pp. 46–50, Feb. 2017, doi: 10.1016/J.VACUUM.2016.11.019.

[46] A. Grabowski, M. Sozańska, M. Adamiak, M. Kępińska, and T. Florian, “Laser surface texturing of Ti6Al4V alloy, stainless steel and aluminium silicon alloy,” *Appl. Surf. Sci.*, vol. 461, pp. 117–123, Dec. 2018, doi: 10.1016/J.APSUSC.2018.06.060.

[47] S. Tsopanos *et al.*, “The Influence of Processing Parameters on the Mechanical Properties of Selectively Laser Melted Stainless Steel Microlattice Structures,” *J. Manuf. Sci. Eng.*, vol. 132, no. 4, p. 041011, Aug. 2010, doi: 10.1115/1.4001743.

[48] “ASTM Compass A479.” [Online]. Available: https://compass.astm.org/EDIT/html_annot.cgi?A479. [Accessed: 16-Apr-2019].

[49] M. Mahmoudi, A. Elwany, A. Yadollahi, S. M. Thompson, L. Bian, and N. Shamsaei, “Mechanical properties and microstructural characterization of selective laser melted 17-4 PH stainless steel,” doi: 10.1108/RPJ-12-2015-0192.

[50] S. R. Ch, A. Raja, P. Nadig, R. Jayaganthan, and N. J. Vasa, “Influence of working environment and built orientation on the tensile properties of selective laser melted AlSi10Mg alloy,” *Mater. Sci. Eng. A*, vol. 750, pp. 141–151, Mar. 2019, doi: 10.1016/J.MSEA.2019.01.103.

[51] H. Wang, M. Nakanishi, and Y. Kawahito, “Effects of welding speed on absorption rate in partial and full penetration welding of stainless steel with high brightness and high power laser,” *J. Mater. Process. Technol.*, vol. 249, pp. 193–201, Nov. 2017, doi: 10.1016/j.jmatprotec.2017.06.014.

[52] T. Wang, Y. Y. Zhu, S. Q. Zhang, H. B. Tang, and H. M. Wang, “Grain morphology evolution behavior of titanium alloy components during laser melting deposition additive manufacturing,” *J. Alloys Compd.*, vol. 632, pp. 505–513, May 2015, doi: 10.1016/j.jallcom.2015.01.256.

[53] B. Liu, Q. Yang, and Y. Wang, “Intereaction and intermetallic phase formation between aluminum and stainless steel,” *Results Phys.*, vol. 12, pp. 514–524, Mar. 2019, doi: 10.1016/J.RINP.2018.11.076.

[54] “ASTM Compass.” [Online]. Available: https://compass.astm.org/EDIT/html_annot.cgi?B883+17. [Accessed: 15-Apr-2019].

Appendix

Mechanical properties of MIM preforms

Tests were carried out on monolithic tensile bars produced through the MIM process with Sandvik, EOS and a blend of Sandvik and EOS powders to determine their mechanical properties.

Additionally, the impact of a heat treatment, commonly used to release the stresses induced during the PBF process, was applied on monolithic MIM preforms to study its effect on their mechanical properties. The heat treatment involved heating the MIM part to 900°C and then holding the temperature for 90min in the furnace environment.

The MIM bars were produced with the three different powders but only the Sandvik powder led to sintered parts with adequate properties. The particle size of the other powders was too large and therefore due to the separation effects the MIM bars were deformed and had undesired weld lines. It is important to note that both defects are unacceptable for mechanically loaded components.

Five MIM bars produced with each powder composition were analyzed to investigate their yield strength, ultimate strength and elongation, i.e. $R_{p0.2}$, R_m, and A%, respectively. Figure A1 depicts the tensile curves of the five MIM bars produced with the Sandvik powder. The overlay of curves is the result of their consistent mechanical properties and hence the good reproducibility achievable with the MIM process. The curves for the MIM bars produced with other two powders had shown the same consistency.

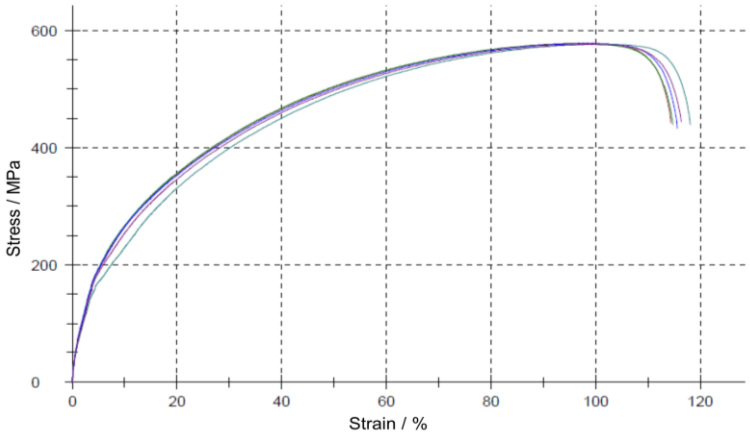

Figure A1: Tensile test curves of 5 MIM bars produced with the Sandvik powder.

The results obtained with the three powder compositions are provided in Table A1. The results show good reproducibility with marginal deviations, only. It can be stated that all MIM 316L bars irrespective of the used powders to produce them conform to ASTM A 420 and ASTM B883 standards in regards to R_m and elongation results [54]. However, only the MIM bars produced with the Sandvik powder demonstrated a yield stress that conforms to the 316L standards. After undergoing the PBF heat treatment, all MIM bars irrespective of the used powders had yield stress that conformed to the standard, especially their yield stress increased and the elongation decreased approximately 20% and 30%, respectively.

Table A1: Results of the tensile tests carried out on MIM bars.

		$R_{p0.2}$ [MPa]	R_m [MPa]	A [%]
EOS MIM	As-built	168 ± 5	503 ± 0,5	87 ± 4
	With heat treatment	186 ± 8	524 ± 1	86 ± 2
EOS/Sandvik MIM	As-built	163 ± 5	549 ± 0,5	90 ± 4
	With heat treatment	213 ± 7	539 ± 1	72 ± 1
Sandvik MIM	As-built	175 ± 9	577 ± 0,8	104 ± 0,7
	With heat treatment	216 ± 7	539 ± 1	72 ± 1
316L Standard ASTM A 420		172	485	40

It should be noted that the heat treatment induced an embrittlement for the samples produced with Sandvik and the blend of EOS/Sandvik powders. This embrittlement can be the result of the precipitation of the sigma phases out of the delta ferrite phases at the grain boundaries. The MIM bars produced with the Sandvik powder had a more pronounced precipitation than those produced with the EOS powder. This can be explained with the differences in their compositions although both are within the range of the 316L standard specification. The

composition of the EOS powder includes Cr, Mo and Si that are used to stabilise the austenitic phases better than the Sandvik powder. Therefore, the precipitation of the delta ferrite phases into the EOS powder was less and thus the precipitation of sigma phases were less, too. Furthermore, the sigma phases precipitate predominantly at elevated temperatures above 900°C, which was exactly the annealing temperature of the applied PBF heat treatment. The MIM parts had better mechanical properties without the follow up heat treatment, besides of undergoing sintering.

The differences in the microstructure of the MIM bars with and without the heat treatment are illustrated in Figure A2(a) and (b). The MIM bars that underwent the PBF heat treatment had a higher concentration of black phases around the grains as shown in Figure A2(a) compared to non-heat treated samples in A2(b). In the latter only small areas of light-grey delta ferrite can be observed between the austenitic grains.

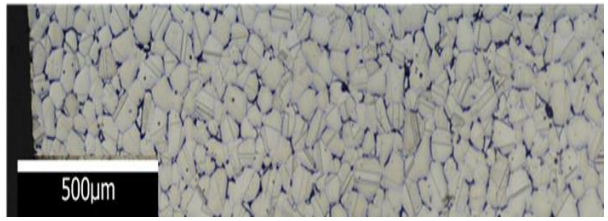

(b)

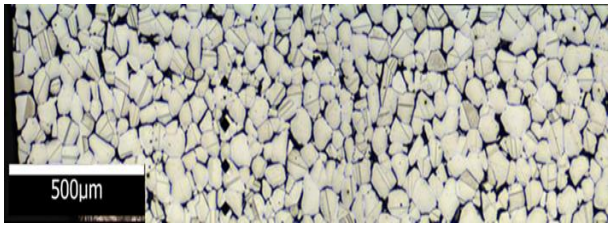

(a)

Figure A2: Microstructure of MIM tensile bar produced using Sandvik powder with and without the PBF heat treatment.

The mechanical properties of all MIM bars produced with and without heat treatment conformed to the 316L standards, while the density the MIM samples produced with Sandvik powder was higher compared to those produced with the EOS powder, 7.92 g/cm³ and 7.62 g/cm³, respectively. However, the mechanical properties of the MIM bars produced with the Sandvik powder were better and also their density was higher and therefore only MIM preforms produced with this powder were investigated further in this research. Especially, hybrid bars manufactured by building PBF sections with the EOS powder on top of MIM preforms produced with the Sandvik powder were investigated further in this research.